






Impact of Concentration on the Hydrothermally Synthesized NiO Nanosheets' Photocatalytic Activity

Haneen Ali Jasim , Nisreen Khalid Fahad *, Sahar Mohammed Ali ,
Baida M. Ahmed  and Osama Abdul Azeez Dakhil 
*Department of Physics, College of Science
Mustansiriyah University, Baghdad, Iraq
Nisreen1994@uomustansiriyah.edu.iq

Received 11 November 2023

Accepted 22 December 2023

Published

In this research, nickel oxide (NiO) peculiar nanosheets with a thickness of less than 50 nm were produced via a low-cost, one-step, safe hydrothermal process. The reaction was conducted with two concentrations of Ni (NO_3)₂·6H₂O (0.01 and 0.03) at 120°C for 3 h. Methylene Blue (MB) dye was used to examine the photoactivity of NiO nanosheet films under sunlight. The prepared NiO nanosheet films were evaluated using XRD, FE-SEM, EDX and UV-visible techniques. Accordingly, (FE-SEM) images confirm that the films synthesized by a hydrothermal method were flower-like nanosheets with a diameter of 33.4–52.7 nm, and the thickness of the NiO film is about 3.629 μm. The average particle size and crystalline structures were estimated using XRD Analysis. However, both films were then exposed to direct sunshine for 80 min. The respective photocatalytic efficiencies of films were calculated to be 85% and 88%. The effectiveness of the photocatalytic degradation for eliminating Methylene Blue (MB) depends on the concentration, proving that the efficiency can be improved by increasing the concentration.

Keywords: Nickel oxide; hydrothermal method; nanosheets; photocatalytic activity; methylene blue; photodegradation.

1. Introduction

The wide variety of physical properties of transition metal oxides (TMOs), along with their potential applications in nanotechnology, microelectronics, materials science and renewable energy, has spurred fundamental research into TMOs in recent years.^{1–4} NiO has attracted interest for its ability to destroy organic contaminants via photocatalytic activity.⁵ This is because NiO, a p-type semiconductor, has a broadband gap of roughly (3.2 eV–4 eV) and excellent transparency.⁶ NiO thin films have low

toxicity, a low cost of manufacture, physical and chemical properties exhibit a high degree of stability, and a powerful capacity to effectively degrade organic contaminants into harmless types such as carbon dioxide (CO₂), water (H₂O) and other similar compounds.^{7–12} To create NiO nanoparticles, a variety of techniques are available, such as the sol-gel method, chemical co-precipitation synthesis, reflux synthesis, microwave synthesis, hydrothermal synthesis, thermochemical approach, etc.^{13–17}

*Corresponding author.

H. A. Jasim et al.

Light's role as a catalyst in the photo-catalysis activity process accelerates a photo-reaction, which is the method by which the organic pollution is broken down by photo-catalysis. No substance used as a catalyst changes or runs out during chemical reactions. The activation of a semiconductor particle (such as NiO, TiO₂, ZnO, and WO₃) to facilitate a redox reaction on its surface is achieved by subjecting it to UV-visible light with an appropriate energy level corresponding to its bandgap. This process is known as Metal-Oxide photo-catalysis. One of the essential requirements for achieving efficient metal-oxide-semiconductor photo-catalysis activity is the appropriate redox potential of the charge pair, or (e⁻ h⁺), which falls inside the photo-catalyst process' bandgap area.¹⁸

The objective of this study is to improve the photocatalytic efficiency of NiO nanostructures. Therefore, it was essential to investigate the impact of synthesis concentration on this feature. Water purification plants could benefit from RB deterioration since it facilitates RB removal.

2. Experimental

2.1. Materials

All of Table 1 chemical ingredients were used directly from the lab without any further purification.

2.2. Synthesis of NiO nanostructures

The hydrothermal technique was utilized to produce the NiO nanosheets. Initially, 80 milliliters of distilled water were stirred to dissolve aqueous solutions of 1% and 3% M nickel nitrate (Ni(NO₃)₂·6H₂O) and 1% and 3% M hexamethylenetetramine (HMT) in 80 milliliters deionized water (DI). These solutions were mixed and kept stirring for 0.5 h. The mixed solution that was acquired was put into a glass autoclave. The prepared substrates were immersed vertically inside the autoclave.

Table 1. Materials used in this work.

Material	Purity (%)	Company
Nickel nitrate hexahydrate Ni(NO ₃) ₂ ·6H ₂ O	99	AAG, Espana
Hexamethylenetetramine HMT, C ₆ H ₁₂ N ₄	99	Hi-media India
Methylene Blue (MB) S3CIN18 H16 C	98.5	Sigma-Aldrich, Germany

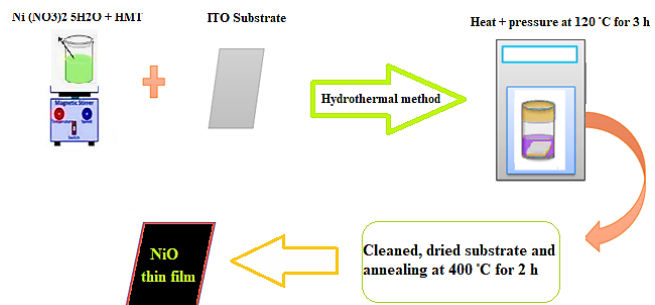


Fig. 1. Graphical scheme for fabrication of NiO thin film using a hydrothermal method with (0.01 and 0.03).

The resultant mixture was transferred and maintained in the oven for 3 h at a temperature of 120°C. After removing the salts from the deposited layer by washing it with distilled water, it was dried on a hotplate at 60°C for 10 min. Subsequently, the film underwent annealing at a temperature of 400°C for 2 h, as shown in Fig. 1.

3. Characterization

A Shimadzu-UV1800 spectrophotometer was utilized to measure UV-visible spectra within the wavelength range of 200–900 nm. To confirm the synthesis of NiO nanostructures, FE-SEM analysis was performed to ascertain the nanostructure's shape and mean particle size. All specimens were studied through FESEM-EDX (Hitachi-S 4160-Japan) in the Chemistry Analysis Center (CAC) of research/Iran-Tehran. X-ray apparatus (model XRD6000; manufacturer: Shimadzu; Japan). The X-ray source utilized was Cu-K α radiation with a wavelength of 0.15406 nm. The device can operate at

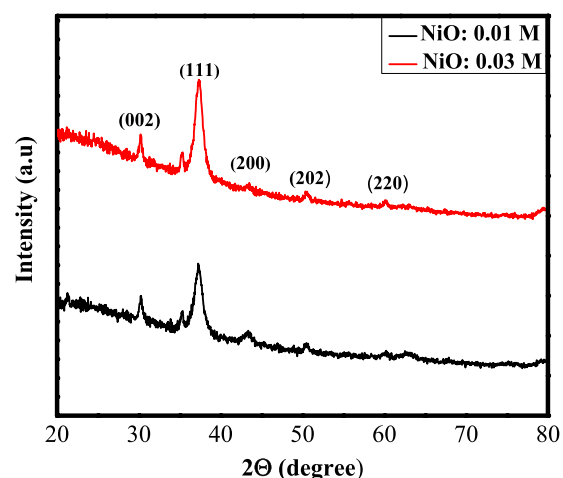


Fig. 2. The XRD patterns of NiO produced at various concentrations (0.01 and 0.03) using a hydrothermal method.



an emission current of 30 mA and a voltage of 40 kV. The specimen is scanned at an angle of (20, 90°).

4. Photocatalytic Degradation

Nanostructures' photoactivity was measured by observing how quickly an aqueous solution of MB

degraded after being exposed to sunlight. The MB solution's absorption peak was measured to be 550 nm across a wide spectrum of wavelengths. For 30 min in the dark, the produced films were immersed in 50 mL of 10 mg/L MB solution to remove surface impurities. Then, spectra of absorption were taken both in the dark and after being

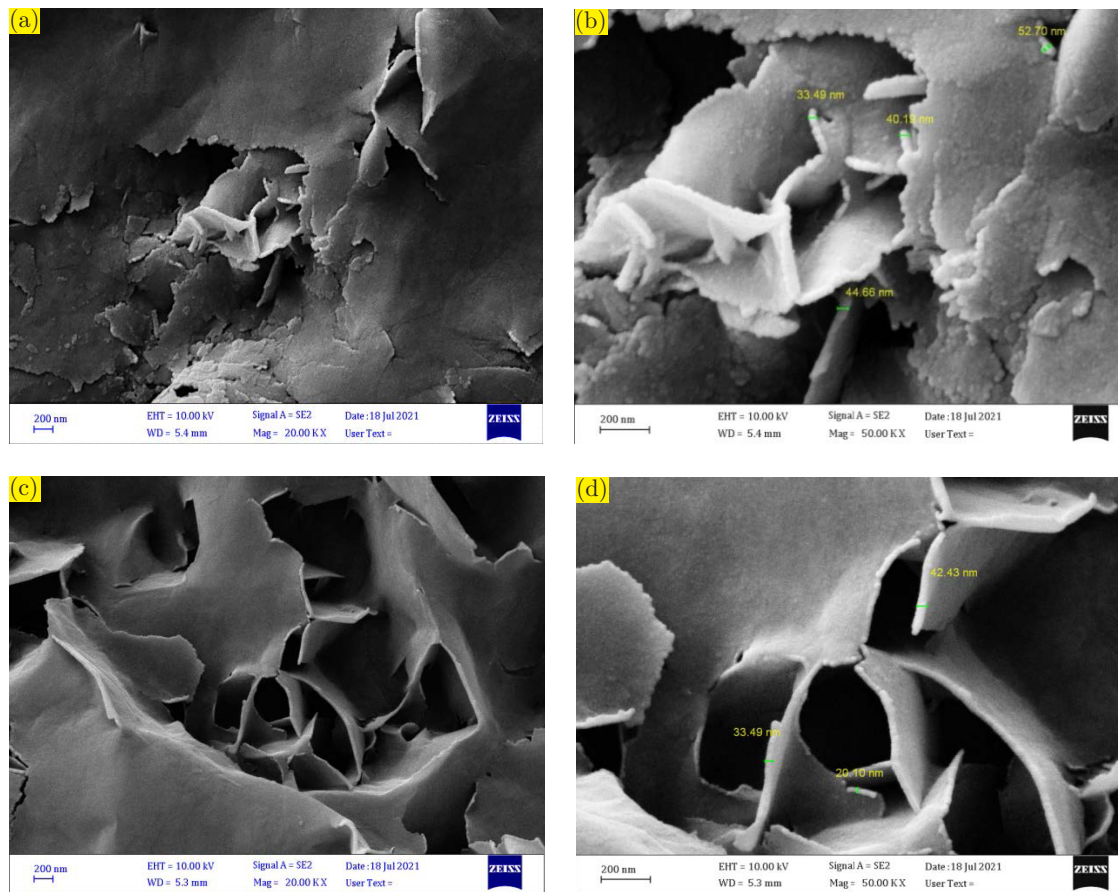


Fig. 3. The FE-SEM Images of NiO thin films prepared with different precursor concentrations, (a, b) samples prepared with 0.01 M, (c, d) with 0.03 M.

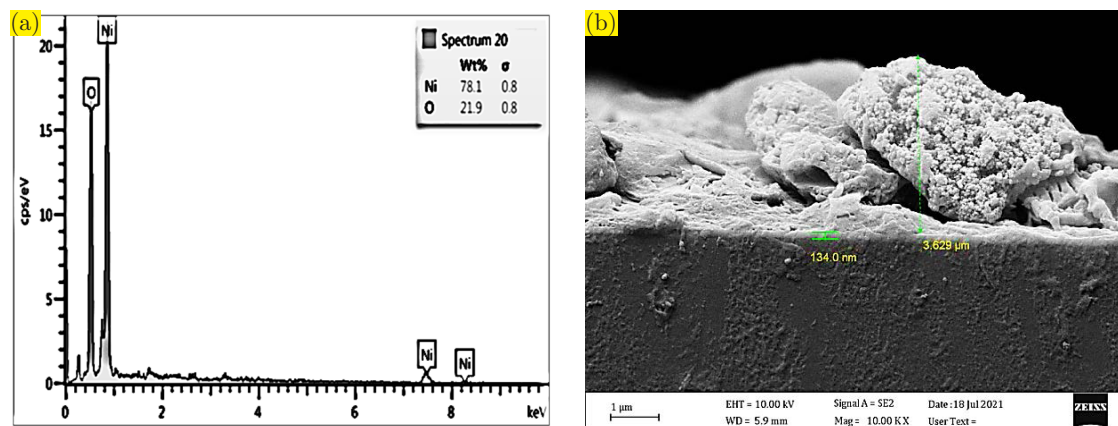


Fig. 4. (a) EDX spectrum and (b) Cross-section image of the NiO thin film for 0.01 M.



H. A. Jasim et al.

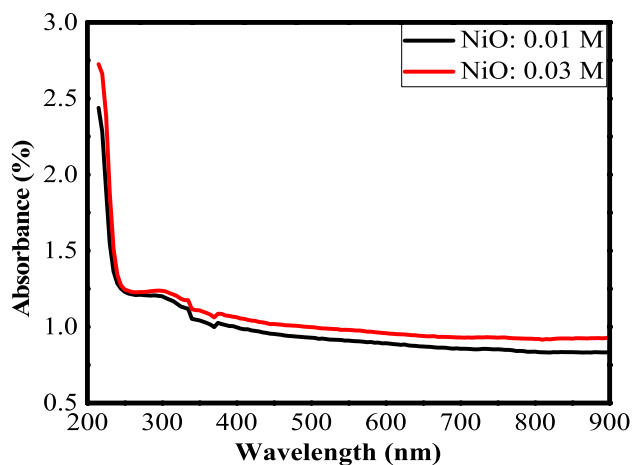


Fig. 5. The UV-Vis absorption of the NiO prepared by 0.01 M and 0.03 M at 120°C for 3 h.

exposed to sunlight for 80 min. The photocatalytic efficiency (P) can be calculated by

$$P = \frac{C_o - C_t}{C_o} \times 100\%, \quad (1)$$

where we consider C_o (mg/L) and C_t (mg/L) as the concentrations of dye before and after light exposure.

5. Results and Discussion

5.1. X-ray diffraction diffraction patterns

Figure 2 displays the XRD diffraction of NiO thin films recorded for two concentrations of (1% and 3%) M. The as-deposited thin film has low crystallinity and exhibits an amorphous structure

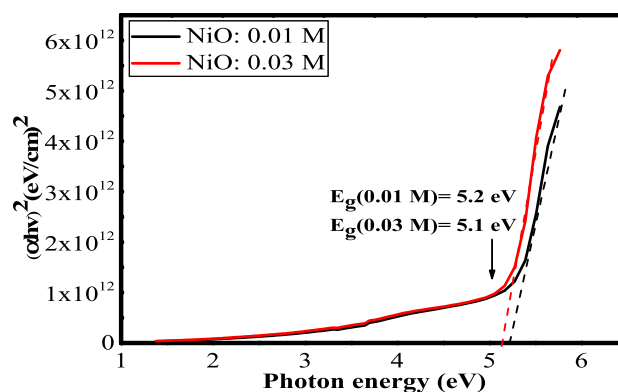


Fig. 6. Tauc plots of direct transitions of NiO prepared by a hydrothermal method with various concentrations (0.01 M and 0.03 M).

at 0.01 M. It's possible that the insufficient NiO film formation at this concentration is to blame.¹⁹ Initiation of crystallization was noticed as precursor concentration was raised from (1% and 3%) M. Based on the X-ray diffraction (XRD) patterns, a singular peak is observed at an angle of $2\theta = 37.24^\circ$, specifically corresponding to the diffraction peak associated with the (111) crystallographic plane. The observation indicates the presence of the NiO phase in its face-centered cubic (FCC) structure, which aligns with the information provided by JCPDS card number 47-1049.²⁰⁻²² No additional impurity peaks were discovered in the XRD patterns in terms of limit detection. The thin film that is observable, which was deposited at a concentration of 3% M, exhibits a more pronounced and well-defined diffraction peak along the (111) crystallographic plane. This suggests a higher degree of crystallization in comparison to other thin films prepared at lower concentrations. Using Scherrer's

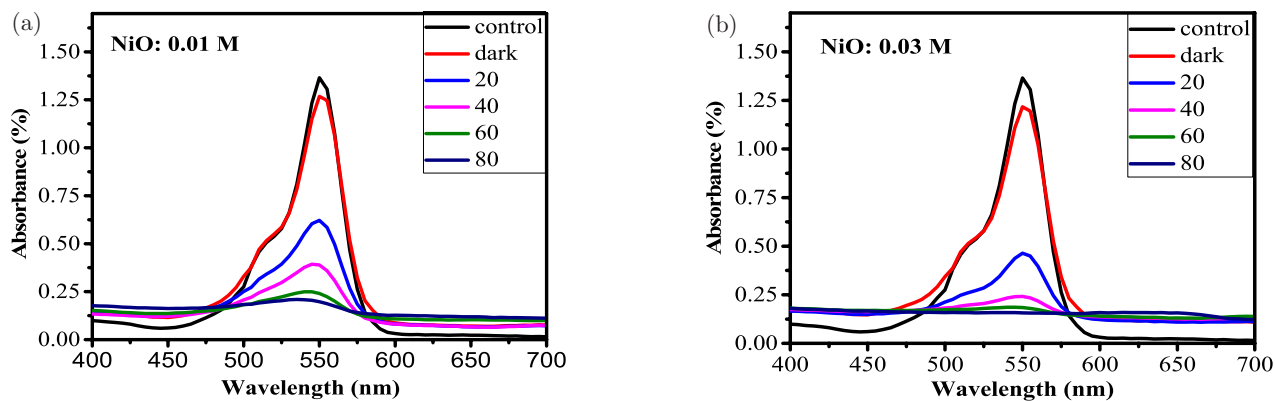


Fig. 7. The UV-Vis photodegradation of MB dye under sunlight by concentrations (a) 0.01 M and (b) 0.03 M.

equation,²³ the films' grain size D for the (111) plane was determined.

$$D = \frac{0.9\lambda}{\beta \cos \theta}. \quad (2)$$

The variable (λ) represents the X-ray wavelength (1.54056 Å) of the incident radiation, whereas (β) denotes the full width at half maximum (FWHM) associated with the diffraction angle (θ). Based on estimations, the average diameters of NiO crystallites in thin films measuring (1% and 3%) M are around 6 and 10 nanometers, respectively.

5.2. FE-SEM images

Figures 3(a)–3(d) show the surface morphologies of specimens with various precursor concentrations (1% and 3%) M. Figures 3(a) and 3(b) show the growth of NiO material on the substrate after a thin layer was constructed using a 1% M precursor concentration. When the concentration of the precursor is raised to 3% M, the substrate is completely covered by nanosheets as seen in Figs. 3(c) and 3(d). The elemental composition of the specimens was identified and quantified with the help of EDX analysis. The EDX spectrum, displayed in Fig. 4(a), demonstrates that the NiO specimen consists of O and Ni, with weights percentages of 21.9%, and 78.1%, respectively. Figure 4(b) also reveals that the typical NiO film has a thickness of 3.629 μm .

5.3. Optical properties

The spectra of optical absorbance from 300 to 900 nm are displayed in Fig. 5. All of the thin films were made using two different amounts of precursors, (1% and 3%) M. As concentration was raised, so was the intensity of the absorption peak. At 3% M, an increase in absorbance and a decrease in transmittance can be attributed to the strong interfacial connection between nanostructures, which allows for the homogeneity and regularity of nanomaterials, or so-called crystalline regeneration. In general, the values of energy gaps rely on the film's crystal structure (disorder and the regularity of the structure).²⁴ According to Tauc's equation,^{25–27} (α) is related to the incident photon energy ($h\nu$).

$$\alpha = \frac{A(h\nu - E_g)}{h\nu}. \quad (3)$$

NiO Nanosheets' Photocatalytic Activity

The optical band gap of NiO films was determined by analyzing the plot of $(\alpha h\nu)^2$ against photon energy. This was achieved by extrapolating the linear portion of the curve to the point where absorption becomes zero, as illustrated in Fig. 6.

6. Photoactivity Degradation

The photocatalytic activities of the NiO nanosheets prepared by a hydrothermal method using two

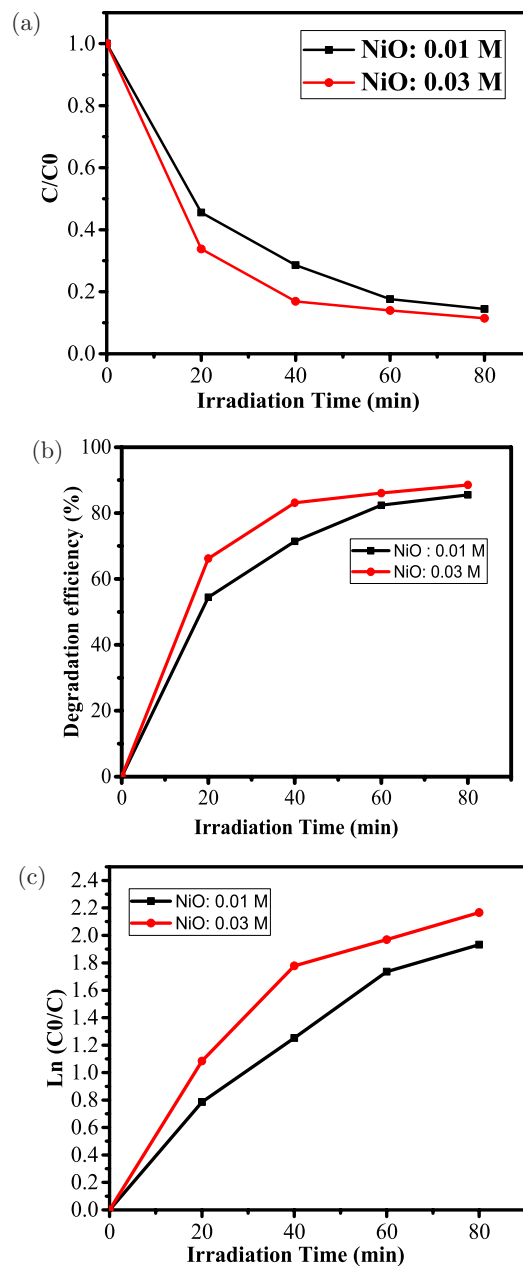


Fig. 8. (a) Time-dependent photodegradation of MB, (b) the degradation efficiency of MB by NiO Nanosheets and (c) first-order kinetics of MB under sunlight.

H. A. Jasim *et al.*

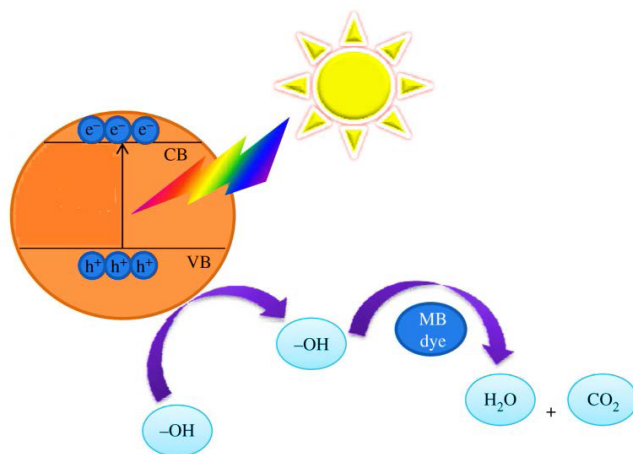


Fig. 9. Mechanism of photocatalytic degradation of methylene blue under natural sunlight using NiO nanostructures.

concentrations (1% and 3%) M are shown in Fig. 7. The maximum values of efficiency of the films prepared by 0.01 M and 0.03 M were calculated to be 85% and 88% for 80 min of exposure to sunlight. However, the maximum difference between the efficiency of Methylene Blue by both concentrations was found to be 11% for 20 min, referring to the dependence of the efficiency on the concentration.

Figure 8(a) depicts the time-dependent photodegradation of (MB), demonstrating that under sunlight, MB decomposition increases. Figure 9(b) demonstrates that after 80 min, NiO nanosheets made at 3% M are more effective than those prepared at 1% M at decomposing MB. Using the concentration-time equation, the pseudo-first-order rate constant, denoted as k (min^{-1}), can be determined by analyzing the slope of the line depicted in Fig. 8(c).

$$\ln \frac{C_0}{C} = kt. \quad (4)$$

The value of k of MB by the nanosheets prepared by (1% and 3%) M is found to be 0.0240 min^{-1} and 0.0260 min^{-1} , respectively. Thus, the photodegradation efficiency of the NiO prepared by 0.03 M is higher. NiO nanosheets would have a far enhanced response if decorated with metallic nanoparticles exhibiting an additional plasmonic absorbance.^{28–30}

7. Conclusions

An easy-to-use and reasonably priced hydrothermal technique was used to develop undoped NiO thin films at 400°C on ITO substrates. The NiO

thin film precursor concentrations ranged from 0.01 to 0.03 M. X-ray diffraction (XRD) structural investigations verify the nanosize structure of the films by showing that an increase in NiO crystallite size near 10 nm occurs as the precursor concentration reaches 0.03 M. FE-SEM images show that at a concentration of 0.03 M for the precursor, the substrate is entirely coated with NiO. The photocatalytic activities of the NiO nanosheets are tested on MB using two concentrations 0.01 M and 0.03 M. The highest value of efficiency for degradation of MB is using 0.03 M. Thus, the photocatalytic efficiency is increased with an increase in concentration.

Acknowledgments

The authors express their gratitude for the financial assistance provided for this research by the Department of Physics, College of Science, Mustansiriyah University, Baghdad, Iraq.

ORCID

Haneen Ali Jasim  <https://orcid.org/0009-0004-7546-8123>
 Nisreen Khalid Fahad  <https://orcid.org/0009-0009-0286-528X>
 Sahar Mohammed Ali  <https://orcid.org/0009-0001-9287-1422>
 Baida M. Ahmed  <https://orcid.org/0000-0001-9315-1913>
 Osama Abdul Azeez Dakhil  <https://orcid.org/0000-0002-6099-7311>

References

1. K. H. Krishna, O. M. Hussain and C. Guillen, *Res. Lett. Nanotechnol.* **2008**, 1 (2008).
2. J. Wu *et al.*, *New J. Chem.* **38**, 4420 (2014).
3. A. A. Demkov *et al.*, *Microelect. Eng.* **147**, 285 (2015).
4. Z. He and X. Wang, *Cat. Today* **240**, 220 (2015).
5. S. A. Mahmoud, S. Alshomer and M. A. Tarawnh, *J. Mod. Phys.* **2**, 1178 (2011).
6. Z. N. Jameel, A. J. Haider, S. Y. Taha and S. Gangopadhyay, *AIP Conf. Proc.* **1758**, 020001 (2016).
7. A. Haider, R. Al-Anbari, G. Kadhim and Z. Jameel, *MATEC Web of Conf.* **162**, 05006 (2018).
8. S. L. Wang, P. G. Li, H. W. Zhu and W. H. Tang, *Powder Technol.* **230**, 48 (2012).
9. F. A. Harraz, R. M. Mohamed, A. Shawky and I. A. Ibrahim, *J. Alloys Compd.* **508**, 133 (2010).
10. E. Dvininov, M. Ignat, P. Barvinschi, M. A. Smithers and E. Popovici, *J. Hazard Mater.* **177**, 150 (2010).



11. Y. P. Sun, C. J. Murphy, K. R. Reyes-Gil, E. A. Reyes-Garcia, J. P. Lilly and D. Raftery, *Int. J. Hydrog. Energy* **33**, 5967 (2008).
12. M. Alagiri, S. Ponnusamy and C. Muthamizhchelvan, *J. Master Electron* **23**, 728 (2012).
13. A. A. Ezhilarasi, J. J. Vijaya, K. Kaviyarasu and A. Ayeshamariam, *J. Photochem. Photobiol. B Biol.* **164**, 352 (2016).
14. F. T. Thema, E. Manikandan and A. Gurib-Fakim, *J. Alloys Comp.* **657**, 655 (2016).
15. A. T. Khalil, M. Ovais, I. Ullah, M. Ali, Z. K. Shinwari and D. Hassan, *Artif. Cells Nanomed. Biotechnol.* **46**, 838 (2018).
16. A. C. Nwanya, M. M. Ndipingwi, C. O. Ikpo, R. M. Obodo and S. C. Nwanya, *J. Alloys Compounds* **822**, 153581 (2020).
17. S. Thota and J. Kumar, *J. Phys. Chem. Solids* **68**, 1951 (2007).
18. G. Anandha Babu, G. Ravi, M. Navaneethan, M. Arivanandhan and Y. Hayakawa. *J. Mater. Sci. Master Electron* **25**, 5231 (2014).
19. A. K. Mishra, S. Bandyopadhyay and D. Das, *J. Mater. Res. Bull.* **47**, 2288 (2012).
20. J. Sithole, B. D. Ngom, S. Khamlich, E. Manikanadan and N. Manyala, *Appl. Surf. Sci.* **258**, 7839 (2012).
21. B. D. Ngom, T. Mpahane and E. Manikandan, *J. Alloys Comp.* **656**, 758 (2016).
22. Y. Zheng, Z. Pan and X. Wang, *Catal. Chin. J. Catal.* **34**, 524 (2013).
23. I. Van De Polluente and I. Des Polluants, "projekt zee projet mer". *Journal of Nanomaterials*, Volume 2017, (2017). <https://doi.org/10.1155/2017/5204639>
24. J. Wang, P. Yang, X. Wei and Z. Zhou, *Nanoscale Res. Lett.* **10**, 1 (2015).
25. H.-L. Chen, Y.-M. Lu and W.-S. Hwang, *Mat. Trans.* **46**, 872 (2005).
26. R. Y. Mohammed, S. Abdulol and A. M. Mousa, *Int. Lett. Chem. Phys. Astronomy* **11**, 146 (2014).
27. J. Tian, H. Deng, L. Sun, H. Kong, P. Yang and J. Chu, *Thin Solid Films* **520**, 5179 (2012).
28. A. Dakka, J. Lafait, C. Sella, S. Berthier, M. Abd-Lefdil and J. C. Martin, *Appl. Opt.* **39**, 2745 (2000).
29. Z. Y. Nuru, C. J. Arendse, R. Nemitudi and O. Nemraoui, *Phys. B Cond. Matter* **407**, 1634 (2012).
30. O. Nemraoui, C. Sella and A. C. Beye, *Gold Bulletin* **38**, 100 (2005).

